ISSN 1027-5495. Functional Materials, 30, No.2 (2023), p. 171-177.
doi:https://doi.org/10.15407/fm30.02.171

Structure, optical properties and photocatalytic activity of undoped, Nd_2O_3-doped ZnO nanocomposites

***O.V.Chudinovych*[1,2], *D.V.Myroniuk*[1], *L.A.Myroniuk*[1], *O.V.Shyrokov*[1], *I.M.Danylenko*[3]**

[1]Frantsevich Institute for Problems of Materials Science, National Academy of Sciences of Ukraine, 3 Krzhyzhanovsky St., 03142 Kyiv, Ukraine
[2]National Technical University of Ukraine "Igor Sikorsky Kyiv Polytechnic Institute", 37 Peremohy Ave., 03056 Kyiv, Ukraine
[3]V.Lashkaryov Institute of Semiconductor Physics, National Academy of Sciences of Ukraine, 41 Nauky Ave., 03039 Kyiv, Ukraine

Received March, 29, 2023

Nd_2O_3-doped ZnO nanocomposites were obtained by the Pechini method. The influence of the alloying additive content on the microstructure, morphology, optical properties and photocatalytic activity of the powders were examined. The properties of the nanopowders were studied using X-ray phase analysis, scanning electron microscopy (SEM), energy dispersive X-ray spectroscopy. Only one phase is present in the X-ray diffraction patterns of the obtained ZnO powders doped with Nd_2O_3. According to SEM, the synthesized powders have a conglomerate structure. It was established that the morphology of powder particles primarily depends on the content of Nd^{3+} in the material. The photocatalytic properties of ZnO powders doped with neodymium oxide was investigated using methyl orange as a model pollutant. The obtained results indicate that the produced powders are potential candidates for practical application in the photocatalytic degradation of organic compounds.

Keywords: ZnO–Nd_2O_3 nanopowders, zinc oxide, neodymium oxide, photocatalysis, degradation.

Структура, оптичні властивості та фотокаталітична активність нелегованих та легованих Nd_2O_3 нанокомпозитів ZnO, . *О.В.Чудінович, Д.В.Миронюк, Л.А.Миронюк, О.В.Широков, І.М.Даниленко*

Нанопорошки ZnO легованого оксидом неодиму отримано методом Печіні. Вивчено вплив вмісту легуючої добавки на мікроструктуру, морфологію, оптичні властивості та фотокаталітичну активність порошків. Властивості нанопорошків вивчали за допомогою рентгенофазового аналізу, скануючої електронної мікроскопії (СЕМ), енергодисперсійної рентгенівської спектроскопір00. На дифрактограмах отриманих легованих Nd_2O_3 порошків ZnO присутня лише одна фаза. Відповідно до СЕМ, синтезовані порошки мають конгломератну структуру. Встановлено, що морфологія частинок порошків у першу чергу залежить від вмісту Nd^{3+} у матеріалі. Фотокаталітичні властивості порошків ZnO, легованого оксидом неодиму, досліджували за допомогою барвника метилового оранжевого як модельного забруднювача. Отримані результати вказують на те, що отримані порошки є потенційним кандидатом для практичного застосування при дослідженні фотокаталітичної деградації органічних сполук.

1. Introduction

The advantages of using ZnO as a photocatalyst over others are its high quantum efficiency, redox potential, excellent chemical and physical stability, non-toxicity, and low cost of its production technologies [1]. ZnO can be an effective photocatalytic nanomaterial due to the high rate of generation and distribution of photoinduced electrons e^- and holes h^+ [2].

It has been shown in [3–25] that doping ZnO with rare-earth metals (REMs) enhances its photoactive properties. ZnO doped with REM is multifunctional material due to its improved optical, photocatalytic, and magnetic properties. Among REMs, neodymium (Nd) is one of the most widely used elements. Doping with neodymium changes the bandgap of ZnO and can enhance its optical and photocatalytic properties. Metal cations entering the ZnO lattice can shift the energy of the bandgap and make it more or less effective in the photodegradation of organic and toxic pollutants. Photocatalytic properties of materials based on ZnO doped with neodymium (Nd^{3+}) were studied in [5–14].

Research on this topic is relevant and of practical importance. In this work, nanopowders of zinc oxide doped with neodymium oxide were obtained and their properties were studied.

2. Materials and methods

ZnO nanocomposites doped with Nd_2O_3 were obtained by the Pechini method. The method consists in achieving a high degree of mixing of cations in solution, controlled transition of the solution into a polymer gel, removal of the polymer matrix with the formation of an oxide precursor, and maintaining a high degree of homogeneity. Solutions of Zn^{2+} and Nd^{3+} nitrates, obtained by dissolving zinc and neodymium oxides with a content of the main component of 99.99 % in nitric acid, were used as starting materials. Before preparing the initial solutions, neodymium oxide was pre-dried in a muffle at 300°C for 2 hours. Mixtures with different Nd^{3+} contents were prepared from nitrate solutions. The mixtures of nitrate and citric acid solutions were stirred for 1 hour at 80°C. The obtained precursors were dried at 150°C for 24 hours and then subjected to a heat treatment at 800°C.

The samples were analyzed by X-ray powder diffraction on a DRON-3 diffractometer at room temperature (Cu–Kα radiation). Scanning with a step of 0.05–0.1 deg was carried out in the range 2θ = 15–90 deg. The lattice parameters were calculated with the least-square method employing the LATTIC software, with an error of less than 0.0002 nm for a cubic phase. The phase composition was determined using the data of the Joint Committee on Powder Diffraction Standards (JCPDS International Center for Diffraction Data, 1999).

The volume of a unit cell was determined by calculation of cell parameters from the X-ray data [26, 27]:

cubic symmetry: $V_{ek} = a^3$

monoclinic symmetry:

$V_{ek} = a \cdot b \cdot c \cdot \sin\beta$,

hexagonal symmetry: $V_{ek} = 0.866 \cdot a^2 \cdot b$

rhombic symmetry: $V_{ek} = a \cdot b \cdot c$.

Scanning electron microscopy (SEM) was used to assess the homogeneity of the powders. Elemental compositions of the samples were determined by EDXRF X-ray spectral microanalysis using an INCA 450 energy dispersive spectrometer (OXFORD Instruments). Atomic concentrations of elements were determined within the relative experimental error of ~ 0.2 % for the investigated area of 500 μm × 500 μm.

Raman light scattering and photoluminescence spectra were recorded using a Horiba Jobin-Yvon T64000 spectrometer equipped with a CCD detector at room temperature in the inverse scattering geometry. Radiations from a solid-state laser (532 nm) and a He–Cd laser (325 nm) were focused onto the sample using an Olympus BX 41 microscope to study Raman scattering under non-resonant and PL excitation conditions. The diameter of the analyzed spot was 1 μm, and the spectral resolution was 1 cm^{-1}.

The photocatalytic activity of zinc oxide powders doped with neodymium oxide was studied by the decomposition of methyl orange (MO), which was used as a model pollutant. Optical transmittances of MO dyes were investigated on an UV2600i two-beam UV spectrophotometer (Shimadzu) in the range of 300–1100 nm at room temperature. MO in distilled water has two absorption peaks at wavelengths of 270 nm and 465 nm, respectively.

3. Results and discussion

Structural properties

Fig. 1 shows XRD patterns of nanocomposites ZnO doped with Nd_2O_3. Only one phase is present at all samples; peaks corresponding to Nd, Nd_2O_3, NdO, or any additional phases are not observed. This indi-

Table 1. Structural properties of Nd_2O_3-doped ZnO nanocomposites

Sample	Lattice parameters, nm		c/a	Cell volume V, nm^3	APF
	a	c			
ZnO	0.3248	0.5206	1.6	0.0477	0.6138
ZnO-5 % Nd_2O_3	0.3251	0.5206	1.6	0.0476	0.6136
ZnO-10 % Nd_2O_3	0.3250	0.5209	1.6	0.0476	0.6138

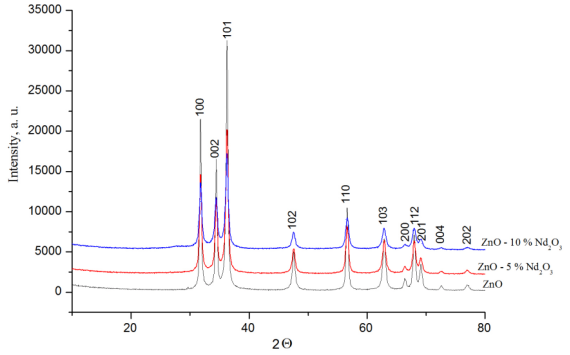

Fig. 1. Diffraction patterns of Nd_2O_3-doped ZnO nanocomposites.

cates the ideal solubility and homogeneity of Nd^{+3} ions in the ZnO lattice.

All the samples have a polycrystalline structure corresponding to the hexagonal phase of wurtzite ZnO. The diffraction patterns were indexed by the ICDD card No. 01-036-1451 (a = 0.3250 nm, c = 0.5206 nm). The main peaks belong to the planes (100), (002), (101), (102), (110), (103), (200), (112), (201), (004), and (202). An increase in the amount of Nd^{+3} in zinc oxide leads to an increase in the lattice period (Table 1). This increase can be explained by the size factor: the ionic radius of Nd^{+3} (0.104 nm) is greater than that of Zn^{+2} (0.074 nm).

Study of morphology and chemical composition

According to SEM, the synthesized powders have a conglomerate structure. In the conglomerate itself, particles are observed whose size does not exceed 100 nm (Fig. 2).

The morphology of powder particles primarily depends on the content of Nd^{3+} in the material. Undoped zinc oxide is characterized by particles of regular shape from 20 to 50 nm, and an average size of 43 nm. Small amounts of single particles with a diameter of 5 nm are also observed (Table 2). The introduction of Nd^{3+} affects the particle morphology and size. The particles begin to acquire a lamellar shape, and their average planar dimensions increases to 64 nm. A more pronounced lamellarity of particles is observed with the addition of 10 % Nd^{3+}.

Table 2. Size of powder particles of Nd_2O_3-doped ZnO nanocomposites

Composition	Size, nm
ZnO	43.1±11
ZnO-5 % Nd^{3+}	64.1±16
ZnO-10 % Nd^{3+}	75.5±25

Raman spectroscopy

Micro-Raman scattering measurements were carried out to study the effect of Nd^{3+} doping on the structural and vibrational properties of ZnO samples.

According to the group theory, ZnO with the wurtzite structure belongs to the space group C^4_{6v} with two formula units per unit cell. The unit cell of ZnO consists of four atoms, each of which occupies the C3v position, leading to 12 phonon branches (three acoustic and nine optical). The irreducible expression of optical phonons is given as $\Gamma_{opt} = A_1 + 2B_1 + E_1 + 2E_2$. A_1 and E_1 are polar modes and can be divided into transverse-optical (TO) and longitudinal-optical (LO) phonons, while B_1 are Raman inactive modes [28]. The oscillation of A_1 phonons is polarized parallel to the c axis, E_1 phonons are polarized perpendicular to the c axis. Each mode corresponds to the band in the Raman spectrum. The intensity of these bands depends on the scattering cross-section of these modes. The nonpolar E_2 modes are Raman active and have two wavenumbers, namely low $E_2{}^{low}$ and high $E_2{}^{high}$, associated with the motion of the zinc (Zn) and the oxygen (O) sublattice, respectively. These strong modes are characteristic for the wurtzite-type lattice and indicate a high degree of crystallinity. The $E_1{}^{LO}$ mode is associated with the presence of oxygen vacancies, Zn interstitials, or their complexes. The $A_1{}^{LO}$ phonon can appear only when the c-axis of wurtzite ZnO is parallel to the sample surface. When the c axis is perpendicular to the sample surface, the $E_1{}^{LO}$ phonon is observed [29].

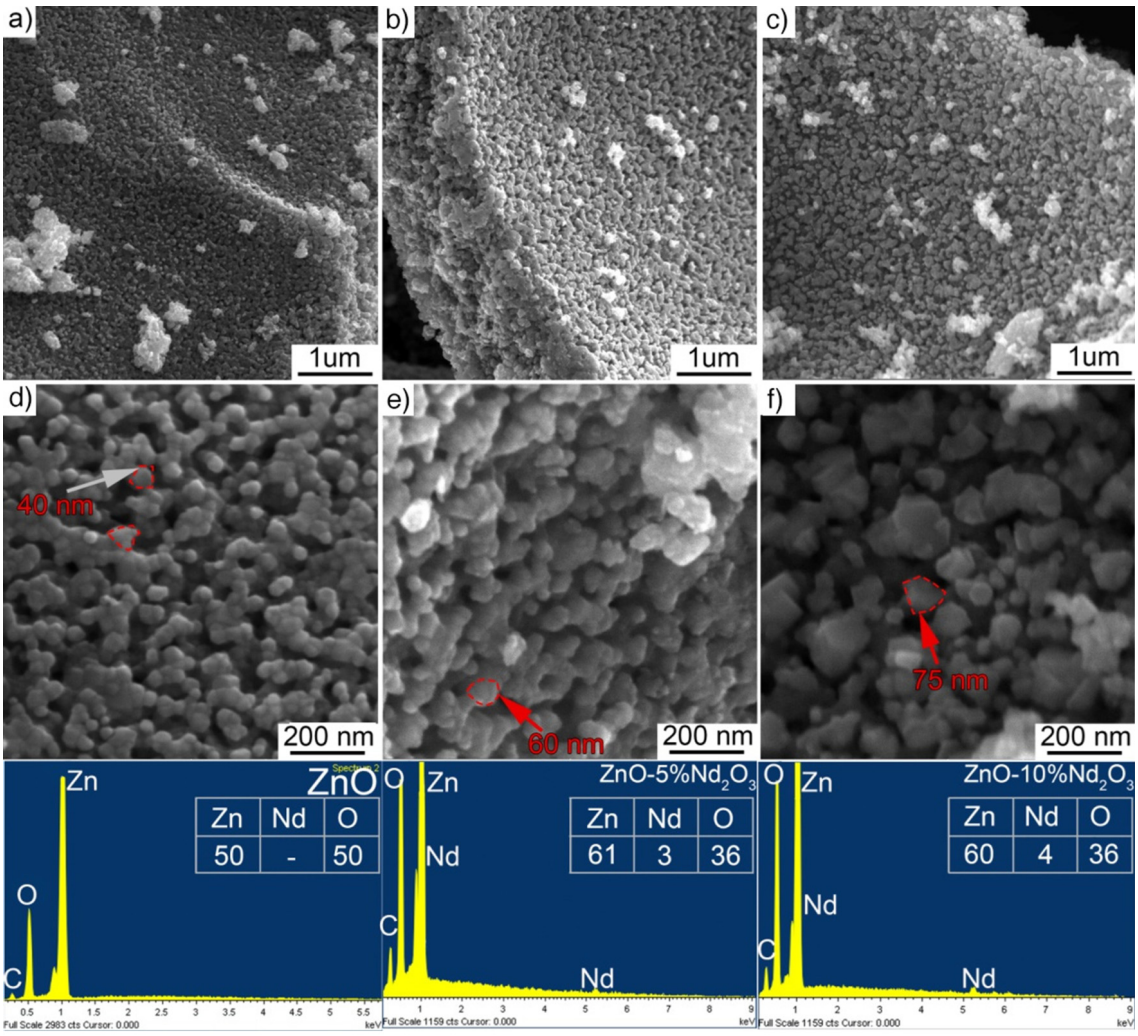

Fig. 2 – Powders of pure zinc oxide (a, d) and doped with 5 % Nd^{3+} (b, e) and 10 % Nd^{3+} (c, e)

Fig. 3 shows Raman spectra of ZnO–Nd_2O_3 nanocomposites. The maxima correspond to phonon vibrational modes of wurtzite ZnO. After peak approximation with the Lorentz function, it was found that the line shape and frequency shift of the E_2^{high} phonon mode depends on the Nd^{3+} concentration. That is, with an increase in the concentration of neodymium, the E_2^{high} phonon mode shifts to a lower frequency and broadens. This behavior may be a consequence of the substitution of Nd^{3+} in the ZnO lattice, which causes a microscopic disorder of the structure in the periodic zinc sublattice. Also, with an increase in the Nd^{3+} concentration, a decrease in the Raman intensity is observed. This structural disorder breaks the translational symmetry of the zinc oxide lattice, leading to fluctuations in the potential of the solid solution ($Zn_{1-x}Nd_xO$), which results in displacement, broadening, and asymmetry of the E_2^{high} mode. A detailed analysis of Raman light scattering spectra confirms that Nd^{3+} ions replace Zn^{2+} positions in the ZnO structure.

Photoluminescence study

Fig. 4 shows the spectra of undoped and neodymium-doped zinc oxide powders. In the PL spectra of ZnO powders a near bandgap edge (NBE) emission around 380 nm and a broadband deep-level emission (DLE) associated with transitions from defects in the range from 450 nm to 800 nm were observed [30–32]. The relatively narrow maximum in the UV region around 385 nm corresponds to the emission during recombination of free excitons [33]. A decrease in the intensity of the NBE emission (Fig. 4) indicates a lower level of radiative recombination of excitons for ZnO doped with neodymium. The decrease in the DLE intensity with doping demonstrates general

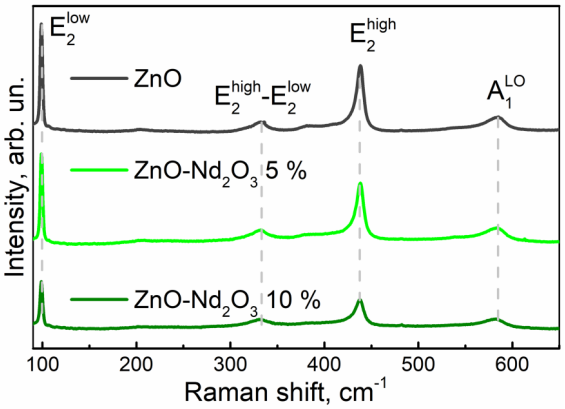

Fig. 3. Spectra of Raman light scattering of Nd_2O_3-doped ZnO nanocomposites

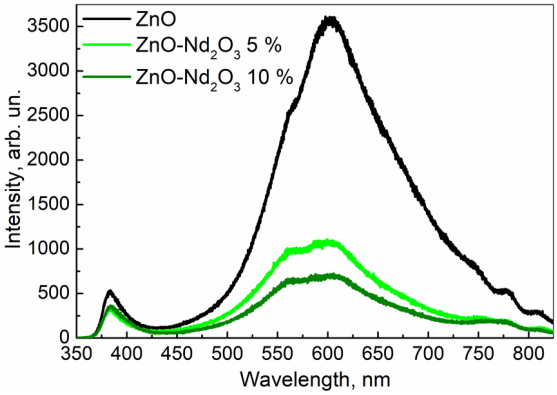

Fig. 4. Photoluminescence spectra of Nd_2O_3-doped ZnO nanocomposites.

inhibition of the PL yield and an increase in the non-radiative recombination processes [34, 35]. The DLE type is usually associated with states of traps — defects in the energy gap, such as vacancies, interstitial atoms, and impurities [36]. The formation of non-radiative defects in the ZnO structure leads to the disappearance of energy levels of the donor type in the forbidden band which take part in the processes occurring during the photoexcitation of the system. The latter causes a decrease in photocatalytic activity.

In addition, a clear shift of the defect emission peak from 605 nm to 560 nm was observed when doping ZnO with neodymium. This can be explained by donor-acceptor recombination or transition from the conduction band to oxygen-related defect levels in the middle of the energy gap. Oxygen can act as a charge accumulation center and provide charge transfer to neodymium ions [37, 38]. Doping with Nd^{3+} affects the PL spectra due to redistribution in the DLE band, which indicates the incorporation of neodymium into the ZnO lattice.

Study of the photocatalytic activity of ZnO and Nd_2O_3-doped ZnO nanocomposites

Photocatalytic activity of undoped and doped with 5 and 10 % neodymium oxide ZnO nanopowders (NC) was studied by the decomposition of an aqueous methyl orange (MO) dye solution. Methyl orange (MO) belongs to the organic azo dyes group, which is widely used in printing, textile, and other industries. Its entry into the environment has a toxic effect on living organisms and, in particular, a carcinogenic effect on humans [39]. In order to study the photocatalytic activity of Nd_2O_3-doped ZnO nanocomposites, the powder catalyst was dispersed in an aqueous solution of MO (10 mg·L^{-1}) under Hg lamp irradiation with power of 200 W during 30, 60, 90 and 120 min. The MO concentrations of in the investigated solutions were determined by measuring of the transmission coefficient at 465 nm.

Fig. 5 shows the UV-VIS absorption spectra of photodegradation of MO dye solutions containing undoped and Nd_2O_3-doped ZnO. After 120 min irradiation, the degradation percentage of MO with undoped ZnO was better than for all the N_2O_3-doped ZnO nanocomposites (NCs).

Fig. 6 presents the photodegradation kinetics of MO dye by ZnO and Nd_2O_3-doped ZnO NCs. The results demonstrate that the Nd-doped samples have a lower photodegradation rate than undoped ZnO. The photocatalytic efficiency of undoped zinc oxide samples consist 99.8 % after 120 min of irradiation. Simultaneously, the photocatalytic activity of ZnO, doped with neodymium oxides does not exceed 13–15 % after 120 min of irradiation. The decrease in the photocatalytic activity of Nd_2O_3-doped NCs can be related to the occurrence of physical defects or with introduced deep bandgap levels between the valence and conduction bands [40].

Photocatalytic reactions proceed with the help of OH· and O^{2-} radicals, formed on the surface of ZnO doped with Nd^{3+}. During photocatalysis, an Nd^{3+} ion absorbs an electron and inhibits electron-hole recombination contributing to the following redox reactions:

$$Nd^{3+} + h\nu \rightarrow \bar{e}(Nd^{3+}) + h^{+}(Nd^{3+})$$

$$Zn^{2+} + h\nu \rightarrow \bar{e}(Zn^{2+}) + h^{+}(Zn^{2+})$$

$$Nd^{3+} + OH^{-} \rightarrow Nd^{2+} + OH^{-}$$

$$OH^{-} + MO \rightarrow \text{Products of photodegradation}$$

$$Nd^{3+} + \bar{e} \rightarrow Nd^{2+}$$

$$Nd^{2+} + O_2 \rightarrow Nd^{3+} + O_2^{-}$$

$$O_2^{-} + MO \rightarrow \text{Products of photodegradation} .$$

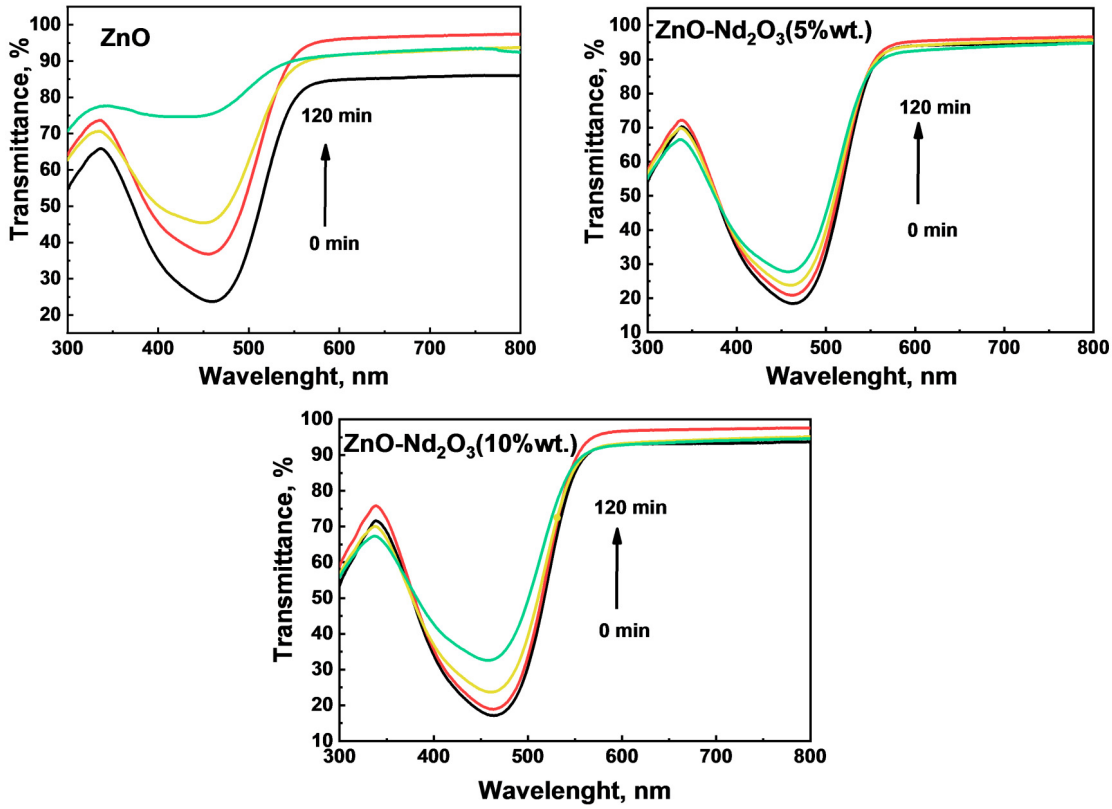

Fig.5. Absorption spectra of Methyl orange (MO) degradation of Nd2O3-doped ZnO nanocomposites at a different time intervals (30, 60, 90 and 120min).

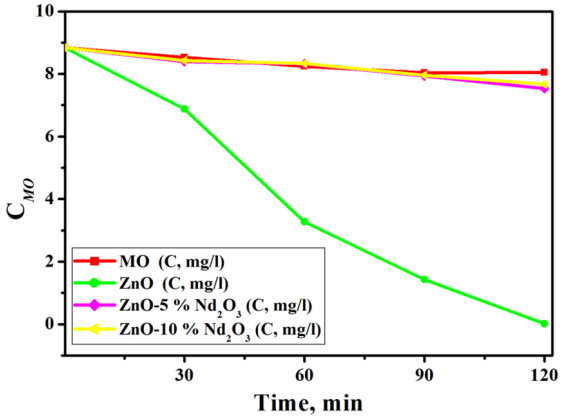

Fig.6. Kinetic for MB degradation of Nd2O3-doped ZnO nanocomposites.

Superoxide ions O^{2-} cause the decomposition reaction mentioned above. The presence of Nd^{3+} ions contributes to the photon absorption of MO, since these ions capture electrons and inhibit electron-hole recombination. An increase in the energy of the band gap has a positive effect on the activity of photocatalysis due to a higher redox potential of photoinduced electron-hole pairs. Thus, the band gap energy and defect states are the determining factor for improving the photocatalytic activity.

4. Conclusions

It is shown that the obtained materials are characterized by a hexagonal structure of wurtzite. An increase in the amount of Nd^{3+} in zinc oxide leads to an increase in the lattice period. According to scanning electron microscopy, the synthesized powders have a conglomerate structure. It was established that the morphology of powder particles primarily depends on the content of Nd^{3+} in the material.

Acknowledge. This work supported by the research project of the NAS of Ukraine "Creation of promising materials based on ZnO doped REE for use in catalysis".

References

1. K.M.Lee, C.W.Lai, K.S.Ngai et al., *Water Res.*, **88**, 428 (2016).
2. G.Kumar, S.Koteswara, K.S.R.Rao, *RSC Adv.*, **5**, 3306 (2015).
3. J.Gupta, P.A.Hassan, K.C.Barick, *Mater Today-Proc.*, **42**, 926 (2021).
4. Y.Zong, Z.Li, X.Wang, *Ceram Int.*, **40**, 10375 (2014).
5. Z.Zhao, J.-L.Song, J.-H.Zheng et al., *T. Nonf. Metal Soc.*, **24**, 1434 (2014).

6. J.Zhang, S.J.Deng, S.Y.Liu et al., *Mater. Technol.*, **29**, 262 (2014).
7. S.Kumar, P.D.Sahare, *J. Rare Earths*, **30**, 761 (2013).
8. O.Yayapao, T.Thongtem, A.Phuruangrat et al., *Mater. Lett.*, **90**, 83 (2013).
9. T.Deepa Rani, K.Tamilarasan, E. Elangovan et al., *Superlattice Microst.*, **42**, 10 (2014).
10. Y.Zhou, S.Lu, W.Xu, *Environ. Prog. Sustain.*, **28**, 226 (2009).
11. P.Logamani, R.Rajeswari, G.Poongodi, *Mater. Sci.*, **1**, 1 (2017).
12. S.B.Satpal, A.A.Athawale, *Mater. Res. Express*, **5**, 1 (2018).
13. J.C.Sin, S.M.Lam, *Chem. Eng. Commun.*, **1**, 1 (2017).
14. A.Samanta, M.N.Goswami, P.K.Mahapatra, *Mater. Res. Express*, **6**, 65 (2019).
15. Z.N.Kayani, B.Amir, S.Riaz et al., *Opt. Mater.*, **109**, 110 (2020).
16. T.Jia, W.Wang, F.Long et al., *J.Alloy Compd.*, **484**, 410 (2009).
17. C.Li, R.Hun, L.Qin et al., *Mater. Lett.*, **113**, 190 (2013).
18. Z.N.Kayani, B.Amir, S.Riaz et al., *Opt. Mater.*, **109**, 110 (2020).
19. N.Clament Sagaya Selvam, J.Judith Vijaya, L.John Kennedy, *J. Colloid Interf. Sci.*, **407**, 215 (2013).
20. P.-T.Hsieh, R.-K.Chuang, C.-Q.Chang et al., *J. Sol-Gel. Sci. Techn.*, **58**, 42 (2011).
21. T.H.AlAbdulaal, M.AlShadidi, Mai S.A.Hussien et al., *Res. Sq.*, **1**, 1 (2019).
22. P.K.Sanoop, S.Anas, S.Ananthakumar et al., *Arab. J. Chem.*, **9**, 1618 (2016).
23. N.K.Divya, P.P.Pradyumnan, *Mater. Sci. Semicon. Process.*, **41**, 428 (2016).
24. I.S.Boltenkov, E.V.Kolobkova, S.K.Evstropiev, *J. Photoch. Photobio A.*, **367**, 458 (2018).
25. Y.Zong, Z.Li, X.Wang et al., *Ceram. Inter.*, **40**, 10375 (2014).
26. G.B.Bokyi, M.A.Poray-Kosice, X-ray Structure Analysis, Moscow University (1964) [in Russian].
27. S.I.Sydorenko, R.I.Barabash, Modern X-ray Structural Analysis of Real Crystals, Naukova Dumka, Kyiv (1997) [in Ukrainian].
28. T.C.Damen, S.P.S.Porto, B.Tell, *Phys. Rev.*, **142**, 570 (1966).
29. N.Ashkenov, G.Wagner, H.Neumann et al., *J. Appl. Phys.*, **93**, 126 (2003).
30. L.Schneider, S.Halm, G.Bacher et al., *Phys. Status Solidi C.*, **3**, 1014 (2006).
31. D.C.Reynolds, D.C.Look, B.Jogai, *J. Appl. Phys.*, **89**, 6189 (2001).
32. E.G.Barbagiovanni, R.Reitano, G.Franzo, *Nanoscale*, **8**, 995 (2016).
33. J.Yang, R.Wang, L.Yang et al., *J. Alloy Compd.*, **509**, 3606 (2011).
34. L.Honglin, L.Yingbo, L.Jinzhu et al., *J. Alloy Compd.*, **617**, 102 (2014).
35. S.Kumar, P.Sahare, *Mater. Res. Bull.*, **51**, 217 (2014).
36. J.Cajzl, P.Nekvindova, K.Jenickova et al., *Nucl. Instrum Meth. B*, 464, 65 (2020).
37. J.Lang, Q.Zhang, Q.Han et al., *Mater. Chem. Phys.*, **194**, 29 (2017).
38. A.Hastir, N.Kohli, R.C.Singh, *J. Phys. Chem. Solids*, **105**, 23 (2017).
39. K.Golka, S.Kopps, Z.W.Myslak, *Toxicol. Lett.*, **151**, 203 (2004).
40. U.Ruh, D.Joydeep, *J. Hazard Mater.*, **156**, 194 (2008).